On the Preliminary Design and Performance Prediction of Centrifugal Turbopumps – Part 1

Luca d'Agostino,[1 a] Dario Valentini,[1] Angelo Pasini,[1] Lucio Torre,[2] Giovanni Pace[1] and Angelo Cervone[3]

[1] Università di Pisa, Pisa, Italy
[2] Alta S.p.A., Ospedaletto (Pisa), Italy
[3] T.U. Delft, Delft, The Netherlands

Abstract

A reduced order model for the preliminary design and performance prediction of radial turbopumps is illustrated. The model expresses the 3D, incompressible, inviscid, irrotational flow through helical blades with slow axial variations of their pitch and backsweep angles by superposing a 2D axial vorticity correction to a fully-guided forced-vortex flow with axisymmetric stagnation velocity in the meridional plane. Application of the relevant governing equations allows for the closed form definition of the impeller geometry and flowfield in terms of a reduced number of controlling parameters. Mass and momentum conservation are used for coupling the flow leaving the impeller with the 2D reduced order models of the flow in the diffuser and/or the volute, as well as for the evaluation of the mixing losses in the transfer between successive components of the machine. This information completes the geometric definition of the turbopump and determines its ideal noncavitating performance in accordance with the resulting flowfield. As a consequence of the neglect of viscous effects, the slip factor predicted by the present model exceeds those obtained from theoretical/semi-empirical formulas reported in literature for centrifugal pumps, but correctly captures their trend.

1. Introduction

The range of applications of turbomachines is so wide that even relatively minor gains in their efficiency and performance translate into major economic impacts worldwide (Laskshminarayana, 1985). More specifically, in space transportation systems turbopumps represent one of the most crucial components of all primary

[a] The present work has been supported by the European Space Agency under Contract No. 40001025856/10/NL/SFe. The authors would like to express their gratitude to Dr. Giorgio Saccoccia of ESA-ESTEC for his constant and friendly encouragement.

propulsion concepts powered by liquid propellant rocket engines, where stringent limitations are associated with the design of high power density, dynamically stable machines capable of meeting the extremely demanding pumping, suction and reliability requirements of the propellant feed systems (Stripling and Acosta, 1962). In these applications turbopumps often employ an inducer upstream of the centrifugal stage in order to pressurize the flow sufficiently for the main pump, usually one or more centrifugal stages, to avoid unacceptable cavitation, improve its suction performance and reduce the pressure and weight of the propellant storage system.

Significant analogies exist between the impeller geometry of centrifugal turbopumps and compressors, as they rely on similar physical phenomena for raising the pressure of the working fluid. In both cases the structural resistance of the blades under the loads imposed by centrifugal and fluid dynamic forces represents the main limiting factor affecting the structural design of these components. However, in centrifugal turbopumps and compressors the relative importance of these forces is reversed because of the widely different densities of their working fluids. Centrifugal forces prevail in radial compressors, allowing for the adoption of a larger number of slender blades. On the other hand, fewer and thicker blades are used in radial turbopumps in order to sustain the higher bending loads generated by liquids (Brennen, 1994).

Because of their relative simplicity, inviscid methods have been the first to be developed for describing the flow in turbopumps. They can be broadly classified in streamline curvature, potential and Euler methods.

Streamline curvature methods essentially derive from the original idea of Wu, 1952, of projecting the equations for the steady, ideal flow relative to the impeller on two pseudo-orthogonal meridional and circumferential surfaces. The 3D flow problem is thus split into two coupled two-dimensional flow problems in the hub-to-shroud and blade-to-blade planes, which are then solved by a number of methods, including finite differences, finite elements and (again) streamline curvature methods (Senoo and Nakase, 1971; Bosman and El-Shaarawi, 1976; Adler and Krimerman, 1978; Hirsch and Warzee, 1979).

Potential methods generate the solution of the irrotational ideal fluid equations for the velocity potential, in most cases by means of finite differences, finite elements, or finite volume algorithms in two or three dimensions. They are relatively fast, intrinsically accurate, and can treat unsteady flow problems precisely both in two and three dimensions. However, the hypotheses of irrotationality severely their applicability to turbomachinery since the relative flow in impellers is necessarily rotational, and even for stationary elements inlet flow prerotation is a common occurrence.

Finally, Euler methods use similar numerical approaches to the solution of the ideal fluid equations, without necessarily requiring the flow to be irrotational.

Clearly, all inviscid methods are inherently uncapable to account for real fluid effects and dissipative phenomena such as turbulence, boundary layers, separation, flow reversal, secondary flows. In order to address these aspects of turbomachinery flows, viscous methods must be used, which can be generally divided in distributed-loss, boundary layer and Navier-Stokes methods.

Distributed-loss methods are based on the idea of correcting the inviscid flow models by accounting for dissipative effects in complex turbomachinery flows on an averaged basis, without detailed consideration of the specific mechanisms and locations where energy dissipation actually occurs (Ainley and Mathieson, 1951; Dunham and Came, 1970; Horlock and Marsh, 1971; Bosman and Marsh, 1974; Kacker and Okapuu, 1982). The appropriate intensity of dissipative effects strongly depends on the operational conditions and must be either deduced from experimental observations or, in more sophisticated models, estimated from the analysis of the various sources of dissipation. Clearly, a sizable amount of information is missed in this intrinsically phenomenological approach. Therefore distributed loss methods are of little or no use when accurate results are required as, for instance, in direct optimization of turbopump design where the sensitivity of the loss model to minor changes of the controlling parameters is indispensible. However, when supported by adequate experimental data, these models represent an economic and rapid way to include in first approximation the global effects of energy dissipation in turbomachinery analyses.

Boundary layer methods are based on Prandtl's original intuition that viscous effects in unseparated flows at high Reynolds numbers are confined to relatively thin layers of the fluid adjacent to the solid surfaces, while the rest of the flow is virtually inviscid. Therefore the flow in the two regions can be studied with separate approaches and the solutions matched together in order to obtain an approximate description of the entire flow field. Boundary layers have been studied extensively and a number of reliable boundary-integral methods exist for their efficient evaluation in the steady 2D case (White, 2006; White and Christoph, 1972). The effects of surface roughness, free stream turbulence and, with some uncertainty, turbulent transition can also be included. The problem of steady viscous/inviscid coupling between the two flow regions can either be neglected in the case of weak interaction, or otherwise treated iteratively in order to satisfactorily match the inner and outer flow solutions (Carter, 1979; Le Balleur, 1981; Whitfield et al., 1981). Boundary layer methods in two dimensions are relatively simple and, in the absence of flow separation, accurate and computationally efficient. On the other hand, extensions to three-dimensional and/or unsteady cases are more difficult and uncertain because of the lack of reliable experimental correlations for solving the integral boundary layer equations and because of the complexity of the computations.

Navier-Stokes methods solve the viscous flow equations, and therefore represent

the most general and comprehensive approach to the analysis of turbopump flows. Current methods typically employ either the Reynolds-Averaged Navier-Stokes (RANS) equations or the Large Eddy Simulation (LES) equations with a suitable turbulence model, in order to reduce the computational requirements to within affordable levels. A very wide variety of algorithms have been proposed in order to better circumvent computational stability problems of Navier-Stokes solvers and improve their overall efficiency. Nowadays they are extensively used in the simulation of turbopump flows, being the most realistic and promising alternative to direct experimentation in the analysis of complex viscous flow phenomena.

The above methods make use of the machine geometry as an input to evaluate its performance (direct methods), and therefore they do not explicitly provide any guidance for its most efficient design. Their use to this purpose in direct optimization loops is very severely limited by the prohibitive cost of exhaustive nonlinear searches over the large number of free parameters that should conceivably be used to define the geometry of the machine in a sufficiently general way. This is especially the case when the complexity and time requirements of each computation are increased for improving the accuracy of the results. Inverse (or indirect) methods, on the other hand, yield the optimum geometry of the machine under given requirements but, in spite of their theoretical appeal, the difficulties associated with their application to the generation of realistic turbopump geometries still make them rather impractical.

The use of the above methods for the fluid dynamic design of the blading and flow path in centrifugal turbopumps satisfying assigned requirements and specifications typically starts by sizing the main components and evaluating their performance by means of simplified 2D or quasi-1D flow models, possibly with empirical corrections for major sources of flow losses (Laskshminarayana 1985). A first approximation of the machine geometry is then generated and a relatively elaborate optimization process is carried out, usually with the objective of attaining maximum efficiency within the assigned specifications, requirements and operational constraints. At increasing levels of complexity, this process may involve the use of blade-to-blade and/or hub-to-tip flow models, boundary layer calculations, and three-dimensional inviscid/viscous, steady/unsteady numerical simulations. The real-fluid performance of the machine is evaluated from the flow velocity field by accounting for energy losses either explicitly, using empirical correlations of specific databases, or indirectly from boundary layer computations or viscous flow simulations. Finally, the geometry of the blade channels and of the other components are iteratively modified in order to attain the desired velocity/pressure distribution along the flow path, reduce residual spurious and/or detrimental effects, and optimize the overall performance of the machine.

Generally desirable features of practical methods for preliminary design of mixed-flow centrifugal turbopumps are:

- the capability of defining the geometry of the machine consistently with the principles of its operation and of predicting its performance in terms of a relatively small number of significant parameters;
- rapid execution times and adequate accuracy and sensitivity to geometrical changes, for more effective iterative optimization of the machine.

The observation that none of the above methods satisfactorily matches these requirements justifies the search for more efficient alternatives. In this context, the development of accurate 3D, closed-form, reduced-order models capable of jointly predicting the geometry and performance of radial impellers and turbopumps is of particular interest to rocket engineers in their search for effective, rapid and possibly accurate tools for the preliminary design of these machines. However, no such model has been proposed so far, mainly due to the difficulty of adequately describing the 3D flowfield through the impeller. Hence, even today turbopump designers still refer to simple "rules of thumb" or the general indications of specific manuals (Douglass, 1973) for the preliminary definition of their machines.

In rocket engine turbopumps the attainment of high power/weight ratios is invariably obtained by running the impeller at the maximum allowable speed and lowest shaft torque. Operation under limited cavitation conditions with lighter – but also more flexible – shafts is therefore tolerated, exposing rocket propellant feed turbopumps to the onset of dangerous fluid dynamic and rotordynamic instabilities (d'Agostino, 2013a; d'Agostino, 2013b). However, the development of cavitation inside the blade channels should possibly be avoided, because the highly compressible and reverberating nature of the flow would greatly promote the onset of potentially lethal self-sustained flow instabilities at frequencies susceptible to become resonant with the flutter oscillations of the impeller blades. The occurrence of this phenomenon in the inducer of the LE-7 engine has actually been identified as the likely cause of the catastrophic failure of the Japanese H-II launcher in November, 1999 (NASDA, 2000a; NASDA, 2000b). It is therefore advisable to design the impellers, both axial and radial, for cavitation to concentrate on the initial part of the blades at all operational conditions. This can be realized if, for any positive value of the inlet flow incidence, the fully-wetted flow pressure on the suction sides of the blades is minimum at the leading edges, and monotonically increasing further downstream. Hence, in particular, the local value of the blade lift vanishes identically at zero incidence, when the stagnation point is located at the leading edge.

These considerations provided the fundamental basis for the selection and justification of the flowfield assumptions adopted by d'Agostino and his collaborators in the development of their closed form methods for jointly defining the geometry and performance of high-head radial inducers (d'Agostino et al., 2008a; d'Agostino et al., 2008b) and mixed-flow impellers (d'Agostino, Pasini and Valen-

tini, 2011) optimized for operation under limited cavitation conditions. Specifically, they first showed that in helical inducers the condition of minimum flow pressure at the leading edges, when associated with the preservation of radially uniform axial flow velocity through the rotor (as commonly required in axial turbomachines), results in a functional relation between the local values of the blade angle and hub radius. Later, with a similar approach d'Agostino, Pasini and Valentini (2011) demonstrated that, when applied to mixed-flow centrifugal impellers, the same condition links together the axial variations of the blade pitch and backsweep angle.

The present formulation of the preliminary design of mixed-flow turbopumps represents therefore the natural extension of the earlier model developed by some of the authors for the simultaneous geometry definition and noncavitating performance prediction of high-head axial inducers for liquid propellant rocket engine feed systems. This model has been used for designing several tapered-hub, variable-pitch inducers with different hydrodynamic features, and successfully validated in a series of dedicated characterization experiments (d'Agostino et al., 2008a; Torre et al., 2011; Cervone et al., 2012; Pace et al., 2013; Torre et al. 2009).

More specifically, the present approach is suitable for application to centrifugal pumps with uniform axial inlet flow, variable impeller tip/hub radii and helical blades with slow axial changes of the pitch and backsweep angles. Following the same approach used in the case of inducers, the 3D incompressible, inviscid, irrotational flow field inside the blade channels is expressed by superposing a 2D cross-sectional axial vorticity correction to a fully-guided flow with axisymmetric stagnation velocity in the meridional plane. This choice allows for a radially uniform axial velocity distribution on each plane orthogonal to the axis of the machine, with the additional advantage of providing hub and tip profiles potentially less prone to develop flow separation. Moreover, the assumed flowfield through the blade channels intrinsically accounts for the influence of slip-flow effects, which are known to be one of the major factors adversely affecting the pumping performance of centrifugal turbopumps.

Due to space limitations, the inclusion of flow losses as first proposed d'Agostino et al., 2012, and the results of dedicated validation experiments on a turbopump designed in accordance with the present model are illustrated in a companion paper of the present volume (d'Agostino et al., 2017). Here, for preliminary assessment of the proposed approach, the slip factors predicted by the present model are compared with those obtained from some of the most popular theoretical/semi-empirical formulas reported in the literature for centrifugal pumps (Stodola, 1927; Busemann, 1928; Wiesner, 1967).

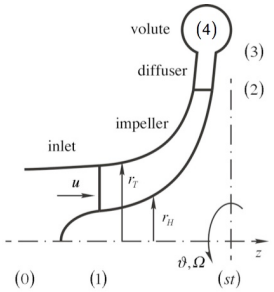

Figure 1. Radial turbopump schematic and nomenclature.

2. Turbopump Flow and Geometry

The present model jointly describes the flow and geometry of the three main components of a radial machine: the impeller, the diffuser and the volute, as schematically indicated in Figure 1.

The radial impeller transfers energy to the working fluid as a consequence of its rotational speed Ω and the hydrodynamic forces developing on its blades. The geometry of its flow channels is defined by the intersection of N blades, with variable helical and backsweep angles γ_h and χ, and the rotational surfaces generated by the axial profiles of the hub and tip radii, r_H and r_T. The exit flow of the impeller is then collected by a vaneless diffuser with constant axial width b_D, and finally guided into the discharge line by a single-spiral volute with elliptical cross-sections, continuously varying in the azimuthal direction from a straight segment at the tongue to a circular cross-section with radius R_4 at the exit.

As mentioned in the introduction, the flow through the machine is considered as incompressible, inviscid and irrotational. For relatively large values of the blade solidity the 3D velocity field inside the blade channels is approximated as the superposition of a fully-guided axisymmetric flow and a 2D axial vorticity correction on each impeller cross-section orthogonal to the centerline. The meridional component of the fully-guided axisymmetric flow is chosen as the velocity field of an incompressible axisymmetric stagnation flow with stagnation plane located at the station (*st*), as illustrated in Figure 1. Perfect mixing is assumed to take place at the exit of the impeller, so that the flow in the diffuser can be considered steady, axisymmetric and axially uniform. Finally, steady axisymmetric flow is also assumed in the volute at design flow rate. Consistently with the ideal nature of the present

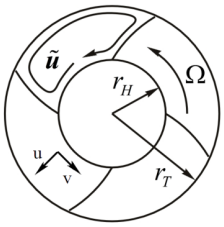

Figure 2. Schematic of the 2D cross-sectional slip flow in the impeller blade channels.

model, mixing losses at the entrance of the diffuser and the volute are neglected, even if they could be evaluated without explicit consideration of real flow effects.

2.1 Impeller Flow and Geometry

In the stated assumptions, the ideal flow through the impeller is held by the continuity and irrotationality equations for the velocity $\boldsymbol{u} = \hat{\boldsymbol{u}} + \tilde{\boldsymbol{u}}$, sum of the (rotational) fully-guided axisymmetric flow field $\hat{\boldsymbol{u}}$, which generates the volumetric flux through the machine and most of its total head rise, and a 2D cross-sectional slip velocity correction $\tilde{\boldsymbol{u}}$ (Figure 2), which does not contribute to the flowrate but is necessary to satisfy the irrotationality condition and decreases the fully-guided head rise.

Fully-Guided Flow and Geometry of the Impeller. With reference to Figure 3, the azimuthal velocity component of the fully-guided flow is expressed by:

$$\hat{v}(r,z) = \Omega r - \hat{w}(z)\tan\gamma(r,z) - \hat{u}(r)\tan\chi(z)$$

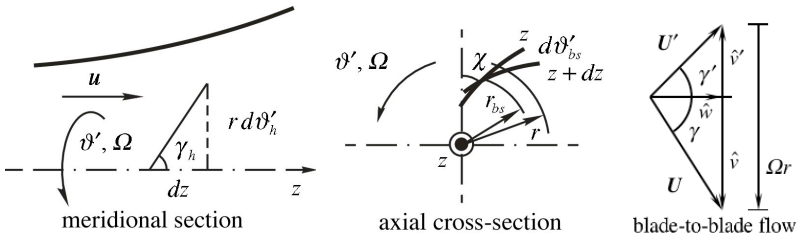

Figure 3. Helical angle in the meridional plane (left), backsweep angle in the axial cross-sectional plane (center) and velocity triangle in the blade-to-blade plane (right).

in terms of the radial and axial velocities $\hat{u}$ and $\hat{w}$, where the angle γ, measured from the axial direction, includes the effects of the axial variations of the helical pitch P_h and of the logarithmic backsweep angle χ of the blades:

$$\tan\gamma = \frac{2\pi r}{P_h} + r\frac{d}{dz}\left[\ln\left(\frac{r}{r_{bs}}\right)\tan\chi\right] = \frac{2\pi r}{P}$$

In this expression $r_{bs}(z)$ is the radius where the azimuthal coordinate ϑ'_{bs} (associated to the axial variation of χ) vanishes (Figure 3) and P is an equivalent helical pitch of the blades accounting for the combined axial changes of P_h and χ.

The relatively narrow range of variation of the radial coordinate $r_H \le r \le r_{\max} = \min\{r_T, r_2\}$ in the blade channels justifies the approximation $\ln r \simeq \ln \overline{r}_\chi = \ln\sqrt{r_H r_{\max}}$, so that P is only function of the axial coordinate z. Hence, in particular, the equivalent pitch of the blades reduces to $P \simeq P_h(z)$ when choosing $r_{bs} \simeq \overline{r}_\chi$.

The 2D slip velocity components on each axial cross-section of the impeller are most synthetically expressed and solved in terms of a scalar axisymmetric stream function $\tilde{\psi}(r', \vartheta', z')$ in the rotating cylindrical coordinates $r' = r$, $\vartheta' = \vartheta - \Omega t$, $z' = z$. Moreover, in the proposed approximation the axial variation of the slip flow is neglected, so that $\partial\tilde{\psi}/\partial z \simeq 0$. Imposition to the assumed velocity field $\boldsymbol{u} = \hat{\boldsymbol{u}} + \tilde{\boldsymbol{u}}$ of the irrotationality condition along the radial, azimuthal and axial coordinates yields:

$$\frac{\partial}{\partial z}\left(4\pi\frac{\hat{w}}{P} - \frac{d\hat{w}}{dz}\tan\chi\right) = 0$$

$$\frac{d^2\hat{w}}{dz^2} = 0$$

$$\frac{1}{r}\frac{\partial}{\partial r}\left(r\frac{\partial\tilde{\psi}}{\partial r}\right) + \frac{1}{r^2}\frac{\partial^2\tilde{\psi}}{\partial\vartheta'^2} = 2\Omega - 4\pi\frac{\hat{w}}{P} + \frac{d\hat{w}}{dz}\tan\chi$$

Successive integration of the azimuthal vorticity and continuity equations, with the conditions $\hat{w}(z_1) = \hat{w}_1$ at the inlet section (1), $\hat{w}(z_{st}) = 0$ at the stagnation plane (*st*) and $\hat{u} = 0$ on the axis, determines the meridional components of the fully-guided flow through the impeller:

$$\hat{w}(z) = \hat{w}_1\frac{z - z_{st}}{z_1 - z_{st}}$$

and:

$$\hat{u}(r) = -\frac{1}{2} r \frac{d\hat{w}}{dz} = -\frac{1}{2} r \frac{\hat{w}_1}{z_1 - z_{st}}$$

which, in turn, define the profiles of the hub and tip radii $r_H(z)$ and $r_T(z)$ as the corresponding streamlines through r_{H1}, z_1 and r_{T1}, z_1.

The blade surfaces are defined by the azimuthal coordinate ϑ'_B resulting from the combined effects of the helical pitch and backsweep:

$$\vartheta'_B = \vartheta'_h + \vartheta'_{bs} = \vartheta'_{B1} - \int_{z_1}^{z} \frac{2\pi}{P_h} dz - \ln\left(\frac{r}{r_{bs}}\right) \tan\chi$$

where ϑ'_{B1} (possibly function of r) is the azimuthal position of the blade at the inlet section $z = z_1$. The adoption of this blade shape yields a forced vortex flow design of the impeller with:

$$\hat{v}' = \hat{v} - \Omega r = -\frac{2\pi r}{P} \hat{w} + \frac{1}{2} r \frac{d\hat{w}}{dz} \tan\chi \sim r$$

It is worth noting that the radial component of the vorticity equation implies that the azimuthal components of the fully-guided flow velocities do not depend on the axial coordinate:

$$\frac{\partial}{\partial z}\left(4\pi \frac{\hat{w}}{P} - \frac{d\hat{w}}{dz} \tan\chi\right) = 0 \quad \Rightarrow \quad \frac{\partial \hat{v}}{\partial z} = \frac{\partial \hat{v}'}{\partial z} = 0$$

Furthermore, integration of this equation in z with the pertinent initial condition at the inlet station (1) determines the backsweep angle $\chi(z)$:

$$\tan\chi = \tan\chi_1 + \frac{4\pi}{d\hat{w}/dz}\left(\frac{\hat{w}}{P} - \frac{\hat{w}_1}{P_1}\right)$$

as a function of the axial schedule of the blade pitch $P(z)$ (or viceversa). For simplicity, in the present analysis a cubic variation of $1/P$ has been assumed, with:

- finite inlet pitch (P_1) and vanishing first and second axial derivatives of $\tan\chi$ at the blade leading edge ($z = z_1$);
- infinite pitch ($1/P_{st} = 0$) at the stagnation plane $z = z_{st}$.

The first condition assures a second order smooth transition of the blading into a helical surface of assigned pitch at the impeller eye, while the second has been imposed to control the angle of the blade root w.r.t. the hub surface at the rotor exit. Although these conditions seemed suitable for first validation of the proposed model, they have not been optimized and further refinements can possibly lead to better results in the generation of more efficient and realistic impeller bladings.

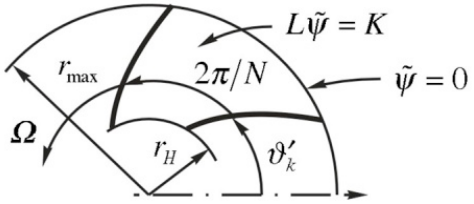

Figure 4. Blade channel cross-section.

Impeller Slip Flow. The Poisson's boundary value problem for the stream function $\tilde{\psi}(r,\vartheta')$ of the slip flow on each axial cross-section of the blade channels (see Figure 4), together with the impermeability condition $\tilde{\psi}=0$ on the boundaries, is transformed in a rectangular domain, where it can be solved in closed form by standard spectral methods (Hildebrand, 1976).

In particular, using as comparison functions the (orthogonal) eigenfunctions of the corresponding homogeneous problem for the Laplace's equation, the solution writes:

$$\tilde{\psi} = \sum_{m=1}^{+\infty}\sum_{n=1}^{+\infty} C_{m,n} \sin\left[n\pi \frac{\ln\left(r/r_H\right)}{\ln\left(r_{\max}/r_H\right)} \right] \sin\frac{(2n-1)N\left(\vartheta' - \vartheta'_{Bk}\right)}{2}$$

with:

$$C_{m,n} = -\frac{\left[2\Omega - 4\pi\hat{w}_1/P_1 + \left(d\hat{w}/dz\right)\tan\chi_1\right] r_H^2 m\left[1-(-1)^m r_{\max}^2/r_H^2\right]}{\left(n-\frac{1}{2}\right)\left[1+m^2\pi^2/\ln^2\left(r_{\max}^2/r_H^2\right)\right]\left[m^2\pi^2\left(n-\frac{1}{2}\right)^2 N^2 \ln^2\left(r_{\max}/r_H\right)/\cos^2\chi\right]}$$

From this solution for $\tilde{\psi}(r',\vartheta')$ the radial and tangential slip velocity components and are readily computed, thus completing the definition of the impeller flow.

2.2 Diffuser Flow and Geometry

In the stated assumptions, the steady, axisymmetric, axially uniform flow in the diffuser is held by the continuity and momentum equations. In order to satisfy the condition of axially uniform flow in the diffuser, perfect mixing of the impeller discharge flow is assumed to occur at the diffuser inlet, with flow velocity equal to the mass-averaged velocity at rotor discharge, station (2). The radial and azimuthal components of the velocity inside the diffuser can then be computed by radially integrating the continuity and azimuthal momentum equations in cylindrical coor-

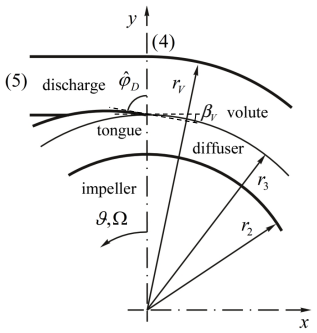

Figure 5. Volute schematic and nomenclature.

dinates. The resulting flow inside the diffuser is characterized by constant axial velocity and log-spiral streamlines with flow angle (φ_D) with respect to the radial direction in a cross-sectional plane. Finally, the flow streamlines through the hub and tip surfaces of the impeller at its discharge station (2) define the lateral surfaces of the diffuser in the meridional plane.

2.3 Volute Flow and Geometry

With reference to Figure 5, the geometry of the spiral volute is designed for alignment of the tongue with the flow leaving the diffuser at nominal operational conditions and smooth transition to azimuthal flow discharge at the exit section, station (4).

The meridional cross-sections of the volute are assumed to be segments of ellipses of width $b_3 = b_D$ at the diffuser exit radius r_3, transitioning from a (degenerate) straight segment at the tongue ($\vartheta = 0$) to a segment of a circle of radius R_4 at the exit of the volute (station 4, $\vartheta = 2\pi$), as schematically illustrated in Figure 6.

In the assumption of axisymmetric flow in the volute at design flow conditions, integration of the azimuthal momentum equation results in a free-vortex distribution of the azimuthal velocity component. The volumetric flux can then be computed on each meridional cross-section of the volute and equated to the radial inlet flow rate from the diffuser. If, in addition, the external radius r_V of the volute is assigned, the above condition fully defines the geometry of the volute as a function of the azimuthal angle ϑ . Here, in particular, the following expression for:

$$r_V = r_3 \exp\left\{\frac{1}{\tan\varphi_D}\left[\vartheta - \frac{\vartheta^{\kappa+1}}{(2\pi)^{\kappa}(1+\kappa)}\right]\right\}$$

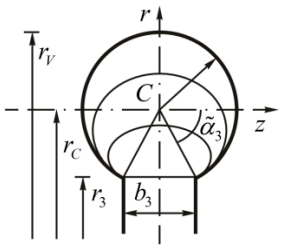

Figure 6. Elliptical meridional cross-sections of the volute.

with:

$$\kappa = \left[1 - \frac{2\pi}{\tan\varphi_D \ln\left(r_{V4}/r_3\right)} \right]^{-1}$$

has been used, corresponding to a smooth variation of the spiral angle β_V of the volute from φ_D at the tongue ($\vartheta = 0$) to zero at the exhaust cross-section ($\vartheta = 2\pi$).

The average flow velocities in the volute have been approximated as

$$\tan\overline{v} = u_3 \frac{A_3}{A_4} \frac{r_{V4}}{r_V} \qquad \text{and} \qquad \overline{u} = \overline{v} \tan\beta_V$$

Finally, in the assumption of a perfect mixing in the outlet duct, the flow at the discharge section (station 5) of the machine is taken uniform with velocity $u_5 = \dot{V} \Big/ \left(\pi R_4^2\right)$.

3. Turbopump Performance

In the present work the pumping performance of the machine has been evaluated neglecting all sources of energy dissipation, consistently with the ideal flow assumption originally introduced to solve for the machine geometry and flowfield. Clearly, the major contributions to fluid dynamic losses (typically arising from viscous and secondary flow effects, turbulent mixing, and flow incidence at the leading edges of wetted surfaces) play a crucial role for realistic performance prediction and optimization of turbopumps. Their inclusion is illustrated in detail in a companion paper of the present volume (d'Agostino et al., 2017), where it is shown to lead to excellent predictions of the measured performance of the machine over a wide range of operation above and below design conditions.

Under the stated assumptions, the impeller is the only element affecting the total pressure of the flow through the machine. Hence, in the reference frame r, ϑ', z rotating with the impeller the (steady) pressure of the (absolutely) irrotational flow in the blade channels is obtained from the Bernoulli's equation:

$$p + \frac{1}{2}\rho \boldsymbol{u}' \cdot \boldsymbol{u}' - \frac{1}{2}\rho \boldsymbol{r} \cdot \boldsymbol{r} = p_{t0}$$

where $\boldsymbol{u}' = \boldsymbol{u} - \boldsymbol{\Omega} \times \boldsymbol{r}$ is the relative velocity and p_{t0} the total pressure on the centerline ($\boldsymbol{r} = 0$) at the upstream station (0).

In the absence of losses the total pressure of the flow downstream of the impeller is uniform. Therefore, using the Euler's equation, the pressure in the diffuser and the volute is computed from the relevant flow velocity $\boldsymbol{u}$ by means of:

$$p + \frac{1}{2}\rho \boldsymbol{u} \cdot \boldsymbol{u} = p_{t0} + \rho \Omega r_2 \overline{v}_2 = p_{t5}$$

where $\overline{v}_2$ is the mass-averaged azimuthal velocity at the impeller discharge.

Finally, with the above results the total head coefficient is expressed by:

$$\Psi = \frac{p_{t5} - p_{t0}}{\rho \Omega^2 r_2^2}$$

In summary, under the stated assumptions and approximations the requirement for axisymmetric stagnation flow in the meridional plane at design conditions determines the profiles of the impeller tip and hub radii, while the irrotationality of the flow completes the geometric definition of the blades by specifying the dependence between the axial schedules of their backsweep and helical pitch angles. The relevant conservation equations and assumptions also parametrically determine the shape of the remaining components (diffuser and volute) and the total head rise of the machine. Both the geometry and performance of the turbopump have therefore been defined in terms of a reduced number of controlling parameters.

4. Model Discussion

In order to illustrate the versatility of the proposed design approach, three examples of pump geometries, indicated as A, B and C and representative of mixed-flow machines with different shape and number of blades, have been generated for suitable inputs of the free design parameters of the model. The 3D renderings of the three pump samples A, B and C and the meridional cross-sections of their impellers are shown in Figures 7, 8 and 9, while Table 1 summarizes their main geometrical characteristics.

Figure 7. 3D rendering of the impeller of the first sample of centrifugal pump geometry (A, left) and meridional cross-section of the impeller (right).

Figure 8. 3D rendering of the second sample of of centrifugal pump geometry (B, left) and meridional cross-section of the impeller (right).

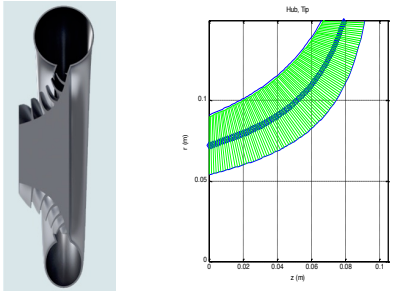

Figure 9. Cut-out rendering of the third sample of centrifugal pump geometry (C, left) and meridional cross-section of the impeller (right).

Table 1. Main characteristics of the three sample geometries of radial turbopumps obtained by means of the present model.

Pump Geometry	A	B	C
Number of Blades	6	8	10
Inlet Tip Radius, (mm)	71.7	60	90
Inlet Hub Radius, (mm)	46	24	54
Stagnation Plane, (mm)	91.7	60	105
Inlet Tip Blade Angle, (deg)	53.1	54	63
Impeller Discharge Radius, (mm)	150	150	150
Diffuser Width, (mm)	12.3	8.1	24.2
Diffuser Discharge Radius, (mm)	180	195	165

Figure 10 illustrates the ideal pumping performance of the sample machines. Since all sources of losses have been neglected, the predicted head characteristics exhibit the linear trend typical of the ideal performance of turbopumps as function of the flow rate.

In the present inviscid flow approximation, the deviation of the flow leaving the impeller w.r.t. the exit angle of the blades is the major source of head degradation in centrifugal turbopumps. In particular, flow deviation at the impeller outlet is mainly due to the slip-flow effect generated by the irrotationality condition and the imperfect guidance of the flow in the blade channels, especially at higher loads (Peterson and Hill, 1992). Of these two effects, the former is actually predicted by

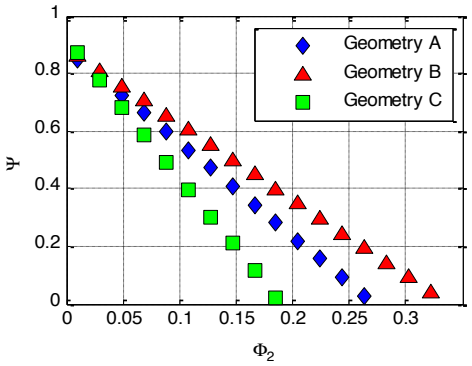

Figure 10. Comparison between the predicted noncavitating performance of the sample turbopump geometries A, B and C.

the present model and can be assessed here, while the latter is rather small in high solidity bladings like those typical of centrifugal impellers with large backsweep angles, and in first approximation can be neglected.

In order to preliminarily assess the performance of the ideal flow model before inclusion of fluid dynamic losses and final validation against experimental data from relevant turbopump geometries, the predicted slip factors have been compared to the results of the theoretical/semi-empirical methods reported in literature for centrifugal pumps (Stodola, 1927; Busemann, 1928; Wiesner, 1967; Dixon, 1978; Ferguson, 1963; Wislicenus, 1947).

In particular, as shown in Figures 11 and 12, the comparison has been focused on the influence of the main parameters affecting the slip factor, such as the number of blades and the exit backsweep angle. The results indicate that the model usually slightly overestimates the slip factor at low number of blades and small exit backsweep angle. However, it is worth noticing that the geometry obtained by the model is more complex than the infinitely thin, logarithmic spiral blades used by Busemann to compute his theoretical slip factors. Moreover, the approximate formula proposed by Stodola provides a reasonable first approximation of the more exact results of Busemann, but underestimates the slip factor when applied to radial impellers with a small number of blades. Both of these methods do not account, even indirectly, for viscous effects.

$$\sigma_B = \frac{A_B + B_B \phi_2 \tan \chi_2}{1 - \phi_2 \tan \chi_2} \qquad \text{Busemann}$$

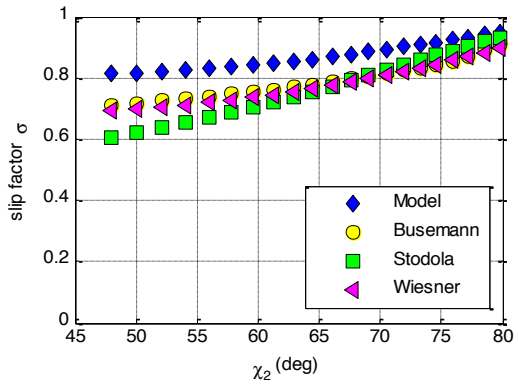

Figure 11. Comparison between the slip factor computed from the model and the available semi-empirical formulas for radial impellers based on the hub and tip profiles of sample geometry C with variable χ_2.

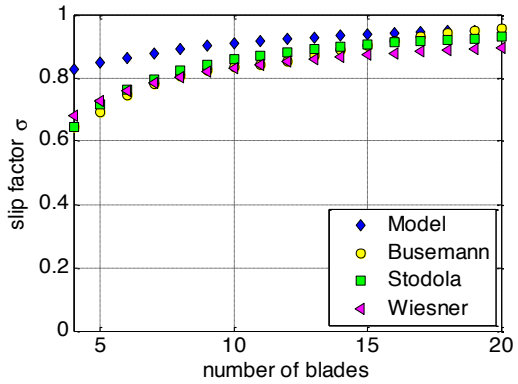

Figure 12. Comparison between the slip factor computed from the model and the available semi-empirical formulas for radial impeller geometries based on geometry C with variable number of blades.

$$\sigma_S = 1 - \frac{0.63\pi/N}{1-\phi_2 \tan\chi_2} \qquad \text{Stodola}$$

$$\sigma_W = 1 - \frac{\sqrt{\cos\chi_2}/N^{0.7}}{1-\phi_2 \tan\chi_2} \qquad \text{Wiesner}$$

On the other hand, the approach proposed by Wiesner is based on empirical slip factor data. It provides better agreement with the experimental measurements and implicitly accounts for the additional contributions of viscous effects. Figures 11 and 12 show that the predictions of the present model well reproduce the trend of Wiesner's results but, not surprisingly, are systematically higher because of the neglect of viscous effects. The introduction of the fluid viscosity decreases the value of the slip factor as a consequence of the acceleration and the additional deviation of the relative flow at the rotor exit induced by blockage and asymmetric boundary layer displacement effects on the two sides of the impeller blades. Both of these effects produce in fact the systematic reduction of the azimuthal component of the absolute flow velocity at the exit of the impeller, and therefore of the head developed by the machine, justifying the observed discrepancy between Wiesner's semi-empirical data and the theoretical results of the present inviscid flow model.

5. Conclusions

The present theoretical model proved to be capable of rapidly and efficiently providing quantitative indications for the geometry definition, the 3D flowfield description, and the prediction of the ideal noncavitating pumping characteristics of radial turbopumps with complex and realistic geometries in terms of a relatively small number of controlling parameters. As illustrated in detail in the companion paper of the present volume (d'Agostino et al., 2017), because of these features the present inviscid flow model is especially suited for easy inclusion of the major forms of flow losses in centrifugal turbopumps and integration in a parametric optimization procedure, with the purpose of generating an effective tool for rapid identification of the machine geometry and performance best satisfying the given set of requirements, specifications and constraints.

The limitations of the model are mostly related to the ideal flow assumption and simplifying approximations introduced in order to attain a practical closed form solution. The experimental validation presented in the companion paper of the present volume (d'Agostino et al., 2017) clearly demonstrates that these limitations can be effectively removed and that major improvements can be gained by introducing the main sources of flow losses in centrifugal turbopumps. Hence, the capability of the present ideal flow model of rapidly and rationally defining the shape of the machine confirms its effectiveness as a design tool of radial turbopumps.

6. Bibliography

Adler, D., and Krimerman, Y. (1978). *The Complete 3-Dimensional Calculation of the Compressible Flow Field in Turbo Impellers*. In J. Mech. Eng.ing Sci., Vol. 20, p. 149.

Ainley, D. G., and Mathieson, G. C. R. (1951). *A Method of Performance Estimation for Axial Flow Turbines*. British ARC, R&M 2974, pp. 923-952.

Bosman, C., and Marsh, H. (1974). *An Improved Method for Calculating the Flow in Turbomachines, Including a Consistent Loss Model*. In J. Mech. Eng.ing Sci., Vol. 16, pp. 23-31.

Bosman, C., and El-Shaarawi, M.A.I. (1976). *Quasi-Three-Dimensional Numerical Solution of Flow in Turbomachines*. IN ASME Paper 76-FE-23.

Brennen, C. E. (1994). *Hydrodynamics of Pumps*. Oxford University Press, 1994.

Carter, J. E. (1979). *A New Boundary Layer Inviscid Interaction Technique for Separated Flow*. In AIAA Paper 79-1450.

Busemann, A. (1928). *Das Förderhöhenverhältnis Radialer Kreiselpumpen mit Logarithmisch-Spiraligen Schaufeln*. Weinheim: WILEY-VCH Verlag GmbH & Co. KGaA.

Cervone, A., Pace, G., Torre, L., Pasini, A., Bartolini, S., Agnesi, L. and d'Agostino, L. (2012). *Effects of the Leading Edge Shape on the Performance of an Axial Three Bladed Inducer*. In 14th Int. Symp. on Transport Phenomena and Dynamics of Rotating Machinery, ISROMAC-14, Honolulu, HI, USA.

d'Agostino, L., Pasini, A., Valentini, D., Pace, G., Torre, L., Cervone, A. (2012). *A Reduced Order Model for Optimal Centrifugal Pump Design*. In: 14th Int. Symp. on Transport Phenomena and Dynamics of Rotating Machinery, ISROMAC-14, February 27th – March 2, Honolulu, HI, USA.

d'Agostino, L. (2013a). *Turbomachinery Developments and Cavitation*. In STO-AVT-LS-206, Paper NBR 12-1, VKI Lecture Series on Fluid Dynamics Associated to Launcher Developments, von Karman Institute of Fluid Dynamics, Rhode-Saint-Genèse, Belgium, April 15-17.

d'Agostino, L. (2013b). *On the Hydrodynamics of Rocket Propellant Engine Inducers and Turbopumps*. In: 6th Intern. Conf. on Pumps and Fans with Compressors and Wind Turbines (IPCF 2013), Sep. 19-22, Beijing, China.

d'Agostino L., Torre L., Pasini A., Cervone A. (2008a). *On the Preliminary Design and Noncavitating Performance of Tapered Axial Inducers*. In ASME J. of Fluids Engineering, Vol. 130, Is. 11, November 2008, pp. 111303-1/111303-8.

d'Agostino L., Torre L., Pasini A., Baccarella D., Cervone A. and Milani A. (2008b). *A Reduced Order Model for Preliminary Design and Performance Prediction of Tapered Inducers: Comparison with Numerical Simulations*. In AIAA Paper 5119, 44th AIAA/ASME/SAE/ASEE Joint Propulsion Conf. and Exhibit, Hartford, CT, USA, July 21–23.

d'Agostino, L., Pasini, A., and Valentini, D. (2011). *A Reduced Order Model for Preliminary Design and Performance Prediction of Radial Turbopumps*. In: 47th AIAA/ASME/SAE/ASEE Joint Propulsion Conference & Exhibit, July 31-August 3, San Diego, California, USA.

d'Agostino, L., Valentini, D., Pasini, A., Torre, L. and Pace, G. (2017). *On the Preliminary Design and Performance Prediction of Centrifugal Turbopumps - Part 2*. In this volume, CISM Courses and Lectures No. 1408, Int. Centre for Mechanical Sciences. d'Agostino L. and Salvetti M.V. Editors. Vien and New York: Springer.

Dixon, S. (1978). *Fluid Mechanics, Thermodynamics of Turbomachinery*. Pergamon Press.

Douglass, H. W. (1973). *Liquid Rocket Engine Centrifugal Flow Turbopumps*. In NASA SP-8109.

Dunham, J., and Came, P. M. (1970). *Improvements of the Ainley/Mathieson Method of Turbine Performance Prediction*. ASME J. Eng. for Power, pp. 252-270.

Ferguson, T. B. (1963). *The Centrifugal Compressor Stage*. London: Butterworths.

Hildebrand, F. B. (1976). *Advanced Calculus for Applications*. Prentice Hall.

Hirsch, C., and Warzee, G. (1979). *An Integrated Quasi-3D Calculation Program for Turbomachinery Flows*. In ASME J. Eng.ing for Power, Vol. 101, p. 141.

Horlock, J. H., and Marsh, H. (1971). *Flow Models for Turbomachines*. In J. Mech. Eng.ing Sci., Vol. 13, pp. 358-368.

Kacker, S. C., and Okapuu, U. (1982). *A Mean Line Prediction Method for Axial Flow Turbine Efficiency*. ASME J. Eng. for Power, Vol. 104, pp. 111-119.

Laskshminarayana, B. (1985). *Fluid Dynamics and Heat Transfer of Turbomachinery*. New York, USA: John Wiley and Sons Inc.

Le Balleur, J. C. (1981). *Strong Matching Method for Computing Transonic Viscous Flows Including Wakes and Separations; Lifting Airfoils*. In La Recherche Aerospatiale, No. 1981-3, English ed., pp. 21-45.

NASDA. (2000a). *Report No. 94*, May 2000

NASDA (2000b). *Report No. 96*, June 2000.

Pace, G., Torre, L., Pasini, A., Valentini, D. and d'Agostino, L. (2013). *Experimental Characterization of The Dynamic Transfer Matrix of Cavitating Inducers*. In 49th AIAA/ASME/SAE/ASEE Joint Propulsion Conference, San Jose, California, USA.

Peterson, C. and Hill, P. (1992). *Mechanics and Thermodynamics of Propulsion*. Reading, (MA) USA: Addison - Wesley Publishing Company.

Senoo, Y., and Nakase, Y. (1971). *A Blade Theory of an Impeller with an Arbitrary Surface of Revolution*. In ASME Paper 71-GT-17.

Stodola, A. (1927). *Steam and Gas Turbines - Volumes I and II*, New York: McGraw-Hill.

Stripling, L., and Acosta, A. (1962). *Cavitation in Turbopumps – Part 1*. In ASME Journal of Basic Engineering, Vol. 84, pp. 326-338, September 1962.

Torre L., Pasini A., Cervone A. and d'Agostino L. (2009). *Experimental Performance of a Tapered Axial Inducer: Comparison with Analytical Predictions*. In AIAA Paper 2009-4955, 45th AIAA/ASME/SAE/ASEE Joint Propulsion Conf. & Exhibit, Denver, Colorado, USA, Aug. 2-5.

Torre, L., Pasini, A., Cervone, A. and d'Agostino, L. (2011). *Experimental Characterization of the Rotordynamic Forces on Space Rocket Axial Inducers*. In ASME Journal of Fluids Engineering, Vol. 133, No. 10.

White, F. M. (2006). *Viscous Fluid Flow*. 3rd Edition, New York, USA, McGraw-Hill.

White, F. M., and Christoph, G. H. (1972). *A Simple Theory for the Two-Dimensional Compressible Boundary Layer*. In ASME J. of Basic Engineering, Vol. 94, pp. 636-642.

Whitfield, D. L., et al. (1981). *Calculation of Turbulent Boundary Layers with Separation and Viscous-Inviscid Interaction*. In AIAA J., Vol. 19, pp. 1315-1322.

Wiesner, F. J. . (1967). *A review of Slip Factors for Centrifugal Impellers*. In ASME J. Eng. For Power, vol. 89, pp. 558-576.

Wislicenus, G. F. (1947). *Fluid Mechanichs of Turbomachinery*. New York: McGraw Hill, 1947.

Wu Chung-Hua. (1952). *A General Theory of Three-Dimensional Flow in Subsonic and Supersonic Turbomachines of Axial, Radial and Mixed Flow Type*s. In NACA, TN 2604.